Diindenopyrazines: Electron-Deficient Arenes

Victor Brosius,[a] Svenja Weigold,[a] Nikolai Hippchen,[a] Frank Rominger,[a] Jan Freudenberg,*[a] and Uwe H. F. Bunz*[a]

Abstract: The syntheses, properties and application of the air-stable electron acceptors, diindenopyrazines **4a**–**g** are reported demonstrating the introduction of functional aryl groups in the 6- and 12-positions. The targets are accessible on the hundred milligram to gram scale. The structure of the aryl groups in **4a**–**g** modulates their solubility, redox potentials and optical properties. The introduction of electron-poor aryl groups to the electron-poor diindenopyrazine backbone reduces the electron affinity to −4 eV, making the compounds attractive as n-semiconductors. A simple organic field-effect transistor of **4e** –without optimization– shows electron transport with a mobility of up to 0.037 $cm^2 V^{-1} s^{-1}$.

Diindenoacenes[1–3] are quinoidal systems[4,5] with the possibility of diradical(-oid) character.[6–8] Such diradicals display attractive magnetic,[9] optical,[10] and theoretical properties.[11] The diradical character is prominent, when the central core is an anthracene.[12] Indenofluorene **1** is a quinoidal closed shell system, as the aromatization energy of benzene – around 21 kcal/mol – is insufficient to enforce the diradical character,[13] while diindenoanthracene **2** displays a diradical ground state (Figure 1a).[12] *N*-Heterocyclic indenofluorenes are sparsely investigated and only recently, Wang et al. described compounds of the type **3** and **4d**.[14] Their electron affinity is increased in comparison to that of **1**. **3** is a triplet diradical while **4d** is a closed-shell singlet, easily understood, as **3** gains two Clar sextet upon "radicalization", while **4d**, analogously to indenofluorene will only gain one of them (Figure 1b).

So far, diradicaloid[12] and closed shell indenofluorene-type compounds[13,15] were applied in organic field effect transistors as ambipolar charge transport systems.[16]

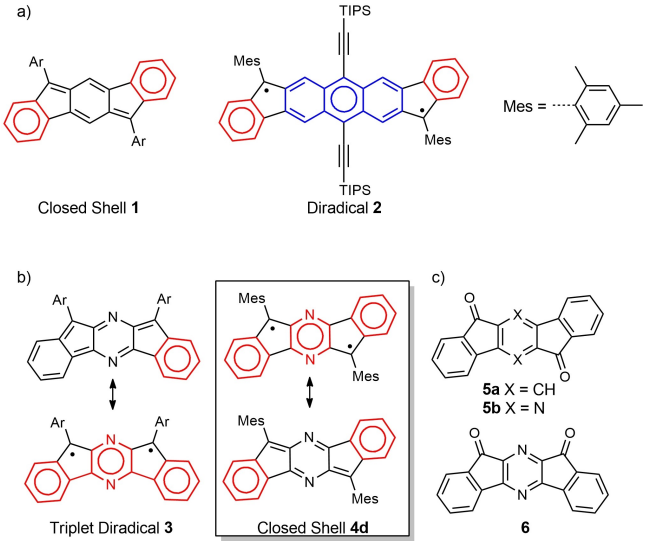

Figure 1. a) Previous work from Haley et al.[12,13] b) Previous work from Pei et al.[14] c) Reactants for the synthesis of **1** (from **5a**), **3** (from **6**), and **4d** (from **5b**).

Compounds **1**, **3** and **4d** were prepared from **5a**, **b** or **6** (Figure 1c) by double addition of an aryl Grignard followed by reductive deoxygenation of the intermediate biscarbinol with $SnCl_2$. Although this is a time-tested method, the yields are variable and for the synthesis of **4d** did not exceed 20%.[14] We are interested in structures of the type **4** and present three different routes that lead to **4** featuring seven different phenyl-substituents. Treatment of **7** with an excess of lithium bis (trimethylsilyl)amide and reaction of the dianion with fluorobenzene, hexafluorobenzene or 4-fluorobenzonitrile gave the compounds **9a**, **e**, **g** after aqueous workup (Scheme 1) . Instead of quenching the in situ generated dianions of **9a**, **e**, **g** with water, addition of chloranil forms **4a**, **e**, **g** in a one pot synthesis in in 30–45% yield as stable crystalline materials without diradical character. For **e** and **g** the S_NAr-mechanism is probably addition-elimination, i.e. associative. For fluorobenzene, an elimination-addition-mechanism cannot be excluded. Variants **b**, **c** and **f** gave inseparable mixtures of compounds, probably due to the presence of an elimination-addition reaction, which gives mixtures of stereoisomers,[17] whereas **d** did not react at all.

Direct arylation by C–H activation of the diindenopyrazine works well for Br–Ar[a–d] in the presence of a Pd^0 source and the biphenyl-based ligand DavePhos giving **9a**–**d** in yields between 25 and 65%. The reaction does not work well with electron-deficient arylbromides, probably due to competing C–H

[a] *V. Brosius, S. Weigold, N. Hippchen, Dr. F. Rominger, Dr. J. Freudenberg, Prof. Dr. U. H. F. Bunz*
Organisch-Chemisches Institut
Ruprecht-Karls-Universität Heidelberg
Im Neuenheimer Feld 270, 69120 Heidelberg (Germany)
E-mail: freudenberg@oci.uni-heidelberg.de
uwe.bunz@oci.uni-heidelberg.de

Supporting information for this article is available on the WWW under https://doi.org/10.1002/chem.202100372

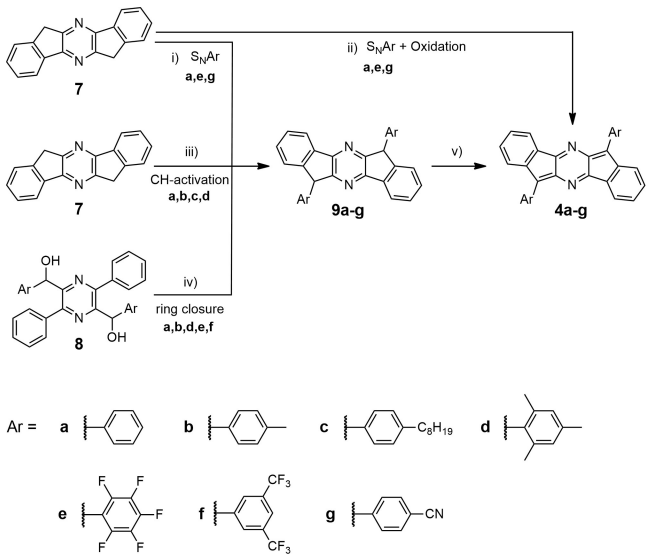

Scheme 1. Synthesis of diindenopyrazines **4a**–**g**. i) LHMDS, F–**Ar**^{a,e,g} in THF, RT, 16 h. ii) one-pot synthesis: LHMDS, F–**Ar**^{a,e,g}, chloranil in THF, RT, 16 h. iii) $Pd_2(dba)_3$, DavePhos, Br–**Ar**^{a,b,c,d}, Cs_2CO_3 in DMAc, 80 °C, 16 h. iv) PPA, 120 °C, 4 h. v) DDQ in PhMe, 100 °C, monitored by thin-layer chromatography or KO*t*Bu, chloranil in THF, RT, 1 h.

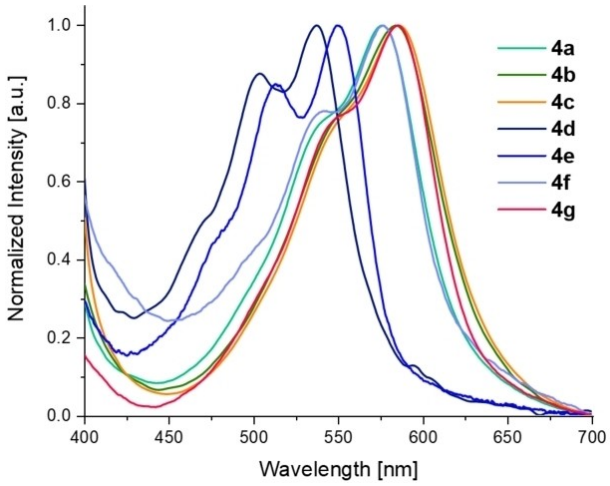

Figure 2. Normalized UV/Vis spectra of **4a**–**g** in CH_2Cl_2.

activation of the aryl bromide. Oxidation of **9a**–**g** with DDQ in toluene at reflux gave moderate yields of **4a**–**g**. The dianions of **9a**–**g**, generated in situ by the addition of KO*t*Bu, were oxidized by DDQ in yields >85%. The third method employs the 2,5-dialdehyde of *para*-diphenylpyrazine. Addition of an aryl Grignard reagent followed by dehydration of the carbinol by polyphosphoric acid gave **9** in 40–70% yield. The S_NAr and C–H activation allow the introduction of aryl substituents that do not survive Grignard formation, necessary to transform **5** or **6** into **1**, **3** or **4**.

On a scale above 50 mg, **4** and **9** were purified by crystallization (exception **4c**, **9c**); but we also note that **5**, the starting material used by Pei et al., is synthesized by oxidation of **7**, which we use directly.[14]

Non-fluorescent compounds **4a**–**g** absorb visible light up to 700 nm, with their absorption maxima λ_{max} ranging between 537 nm (opt. gap 2.31 eV) for **4d** and 586 nm (opt. gap 1.92 eV) for **4b**, **c**. (Figure 2, Table 1). The mesityl and the perfluorophenyl-substituted diindenopyrazines display the most blue-shifted features in their absorption spectra, due to the twisting of the aryl rings with respect to the diindenopyrazine. The other aryl-substituents display more planar geometries, that is, enlarge the π-system. The pyrazine ring allows for a larger degree of planarization, as the peri-hydrogens of the indenofluorenes are absent. The observed red-shift – when compared to the indenofluorenes **1** – is a result of the decreased torsion angle but also due to an electronic effect of the pyrazine. Compared to **1**, HOMO and LUMO levels of **4** are stabilized by the electron-poor pyrazine core (Figure 3).

We obtained single crystalline specimen from **4c** and **4d** (Figure 4); **4c** displays an aryl-diindenopyrazine torsion angle of only 28°, while mesityl substituted **4d** displays an angle of 63°. The larger twist compared to **4c** is caused by steric pressure of the *ortho*-methyl groups and weakens the conjugation of the backbone to the aryl groups (see above). This leads to the already mentioned blue-shift of **4d**, as well as larger HOMO-LUMO/IP-E_A gaps (Table 1). The crystal structure of **4d** has been reported.[14]

Table 1. Experimental and calculated properties of **4a**–**g**.

Compound	$\lambda_{max,\,abs}$ [nm] (CH_2Cl_2)[a]	Opt. gap [eV][b]	$E^{Ox}_{1/2}$ [V][c]	$E^{Red}_{1/2}$ [V][c]	IP [eV][c]	E_A [eV][c]	HOMO [eV][d]	LUMO [eV][d]	HOMO-LUMO gap [eV]
a	576	1.98	0.76	−1.12	−5.56	−3.68	−5.37	−3.43	1.94
b	584	1.92	0.81	−1.18	−5.61	−3.62	−5.28	−3.30	1.98
c	586	1.92	0.85	−1.18	−5.65	−3.62	*	*	*
d	537	2.31	0.93	−1.30	−5.73	−3.50	−5.53	−3.32	2.21
e	550	2.12	–[e]	−0.88	–[e]	−3.92	−6.23	−3.98	2.25
f	577	1.98	–[e]	−0.87	–[e]	−3.93	−6.05	−4.10	1.95
g	586	1.94	–[e]	−0.90	–[e]	−3.90	−5.99	−4.02	1.97

[a] Measurements were performed in CH_2Cl_2. [b] Calculated from $\lambda_{onset,\,abs}$. [c] Oxidation $E^{Ox}_{1/2}$ and reduction $E^{Red}_{1/2}$ half-wave potentials measured by cyclic voltammetry (CV) in CH_2Cl_2 with Bu_4NPF_6 as the electrolyte against Fc/Fc^+ as the internal standard (−4.80 eV) at 0.2 $V\,s^{-1}$. IP and E_A estimated from cyclovoltammetric (CV) measurements [$IP/E_{A\,CV} = -4.80\ eV - E_{Ox/Red}$]. [d] Obtained from quantum-chemical calculations with DFT/B3LYP/def2-TZVP. [e] Not in the accessible stability window of the solvent. * It is not expected that the longer alkyl group of **4c** compared to **4b** has a significant influence on the geometry or energy levels. Therefore, no separate calculation was performed.

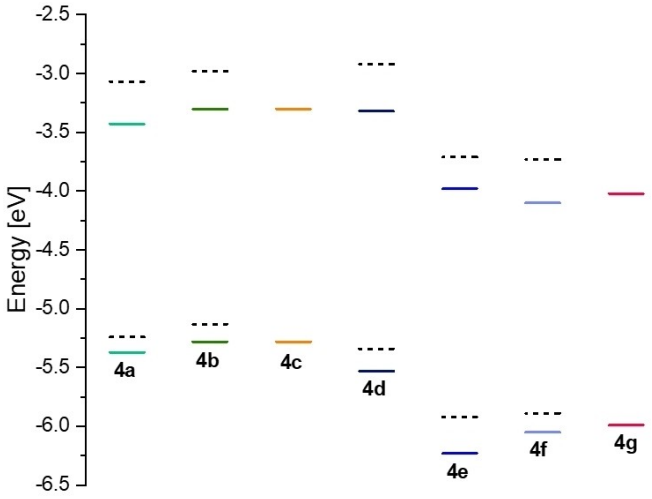

Figure 3. DFT-calculated FMO levels (B3LYP/def2TZVP) of compounds **4a**–**4g**. Dashed lines represent the FMOs of the indenofluorenes **1a**, **b**, **d**–**f**, taken from ref. [12].

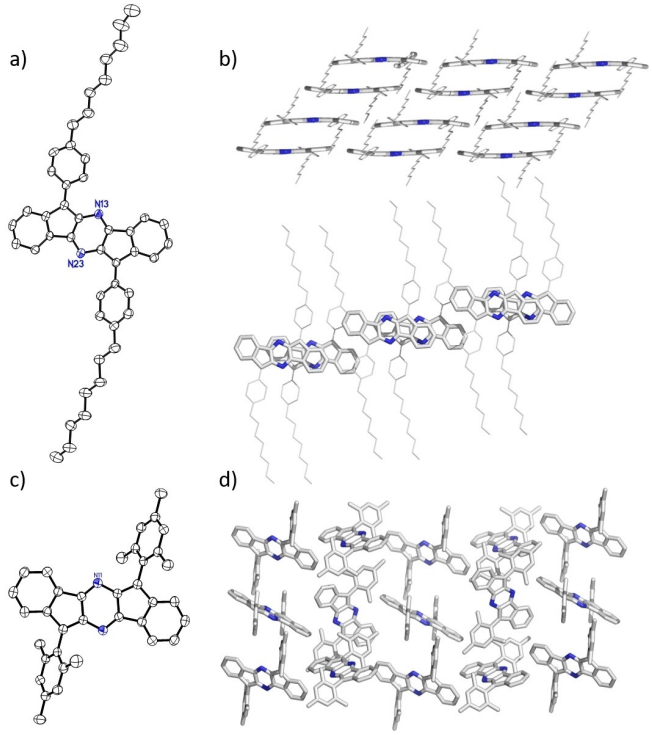

Figure 4. Single crystal structure a), c) and packing b), d) of **4c** and **4d**, respectively.

Both the single crystal structures but also the quantum chemical calculations confirm the quinoidal and non-diradical character of derivatives of **4**. The molecules of **4c** pack in one-dimensional oblique stacks with π–π contacts between parallel diindenopyrazine units; the attached phenyl rings however are oriented perpendicular to those of the adjacent molecules, thus showing CH-π contacts among each other. In contrast, the two independent centrosymmetric molecules of **4d** show no parallel stacking motif in the crystal lattice. In **4c** the distance between the π systems is 3.2 and 3.5 Å, that is, below the van der Waals radii.

We built a transistor with a bottom-gate top-contact geometry of **4e**, due to its sufficient solubility and thus good film forming properties. We used a silicon substrate with successive layers of 100 nm thermally grown silica, solution processed alumina and 12-cyclohexyldodecylphosphonic acid (CDPA) as a self-assembled monolayer to modify the dielectric.[18] A solution of **4e** was drop-cast on the substrate from chloroform (0.38 mg/mL) resulting in a crystalline thin-film (Figure 5a). 40 nm silver was evaporated through a shadow mask to form the contact electrodes. Figure 5b) shows the schematic device architecture. **4e** displays low hysteresis in the transfer curves and is without hysteresis in the output curves, with a top mobility of $\mu_{max}{}^{-} = 0.037\ cm^2V^{-1}s^{-1}$ (Figure 5c,d). The average mobility is $0.022\ cm^2V^{-1}s^{-1}s$ (6 channels, 2 substrates). Compared to the literature known **1e**, which displays ambipolar behaviour with $\mu_{Max}{}^{+} = 7\times10^{-4}\ cm^2V^{-1}s^{-1}$, $\mu_{Max}{}^{-} = 3\times10^{-3} cm^2V^{-1}s^{-1}$ as single crystal transistor the mobility of **4e** is an order of magnitude higher.[13]

Treatment of **4d** with $SbCl_5$ or $NOSbF_6$ in dichloromethane/acetonitrile quantitatively gave the protonated species **4d**$H_2{}^{2+}$, identified by X-ray single crystal structure and UV/Vis spectrum (Figure 6). **4d**$H_2{}^{2+}$ was also obtained by reaction of **4d** with HBF_4. Addition of water to **4d**$H_2{}^{2+}$ re-forms **4d** quantitatively. Oxidation into the radical cation or the dication of **4d** did not occur, probably due to the instability of fluorenyl cation in addition to the destabilizing pyrazine-core and lack of conjugation into the mesityl substituents. For a quinoidal diindenonaphthalene derivative, Haley et al. suggested a higher degree of delocalization of the positive charge compared to that of the negative charge, localized at the fluorenyl position.[19]

We investigated the reduction of **4e** with potassium anthracenide. The radical anion formed easily; its EPR spectrum is in good agreement with the simulated spectrum (see the Supporting Information). The UV/Vis spectrum displays an absorption at 1103 nm (Figure 7). In air, the signal disappears after 90 minutes.

In conclusion, three efficient routes towards diindenopyrazines using S_NAr, C–H activation and ring closure reactions have been presented. Compounds **4** lack diradical character, yet display attractive properties. In particular, **4e** is an n-channel semiconductor, which even in un-optimized proof of concept transistors display mobilities of up to $0.037\ cm^2V^{-1}s^{-1}$.

Experimental Section

Gram scale synthesis of 4e: 6,12-Dihydrodiindeno[1,2-b:1′,2′-e] pyrazine (**7**; 1.50 g, 5.85 mmol, 1.00 equiv.) was dissolved in dry THF (500 mL) and LHMDS (1 M in THF, 35.1 mL, 35.1 mmol, 6.00 equiv.), and hexafluorobenzene (4.36 g, 23.4 mmol, 4.00 equiv.) was added slowly. The reaction mixture was stirred for 16 h at room temperature, and afterwards chloranil (8.63 g, 35.1 mmol, 6.00 equiv.) was added. Recrystallization from chlorobenzene gave **4e** as a dark purple solid. Yield 1.10 g, 1.88 mmol, 32%. ^{1}H NMR ([D_2] tetrachloroethane, 400 MHz): $\delta = 7.59$ (m, 2H), 7.23 (m, 2H), 7.18 (m,

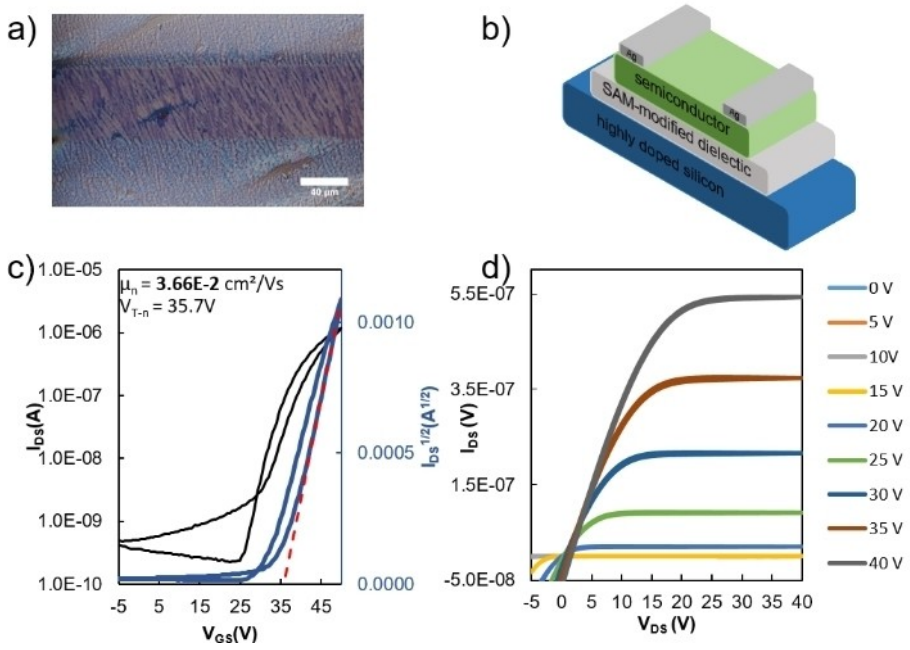

Figure 5. a) Drop-cast film of **4e** from chloroform (0.38 mg/mL), 50× darkfield microscopy. b) Schematic architecture of the device. c) Transfer characteristics of bottom-gate top-contact FET (V_{ds} = 50 V). d) Output characteristics.

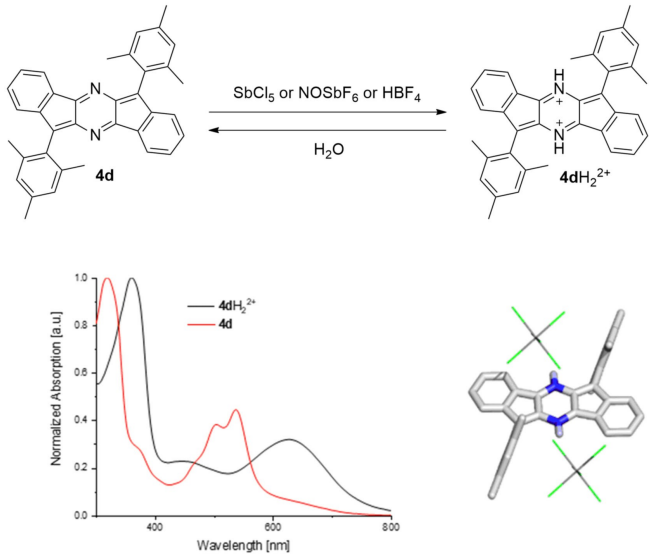

Figure 6. Synthesis, UV/Vis and single-crystal structure of **4d**H_2^{2+} with $SbCl_6^-$ as counterion.

2H), 6.96 (m, 2H) ppm. ^{13}C NMR ([D$_2$]tetrachloroethane, 125 MHz): δ = 165.1, 142.2, 141.8, 138.0, 133.2, 129.7, 129.5, 128.5, 126.3, 123.3, 122.7, 120.2 ppm. IR: $\tilde{\nu}$ 2960, 2920, 2851, 1659, 1632, 1459, 1439, 1425, 1259, 1089, 1060, 1017, 850, 798, 778, 744, 736, 719, 704, 683, 669, 661 cm^{-1}. $\lambda_{max,\ abs}$ = 550 nm, $\lambda_{onset,\ abs}$ = 586 nm. HRMS (DART+): *m/z*: $[M+H]^+$: calcd. for $C_{30}H_8F_{10}N_2^+$: 587.0528; found 587.0596, correct isotope distribution.

Crystallographic data: Deposition Numbers 2058078 (for **4c**), 2058079 (for **4d**), and 2058080 (for **4d**H_2^{2+}) contain the supplementary crystallographic data for this paper. These data are provided free of charge by the joint Cambridge Crystallographic Data Centre and Fachinformationszentrum Karlsruhe Access Structures service www.ccdc.cam.ac.uk/structures.

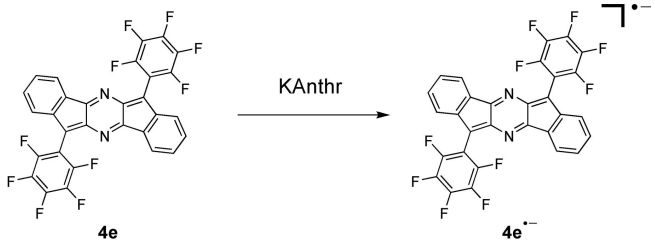

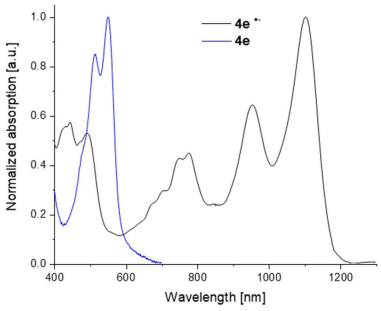

Figure 7. Top: Reduction of **4e** with potassium anthracenide in THF. Bottom: UV/Vis spectrum of **4e**$^{\bullet-}$.

Acknowledgements

Victor Brosius thanks the "Studienstiftung des Deutschen Volkes" for a scholarship. We thank the DFG (SFB 1249) for generous support. Open access funding enabled and organized by Projekt DEAL.

Conflict of Interest

The authors declare no conflict of interest.

Keywords: electron acceptors · organic field effect transistors · quinoidal heteroaromatics · semiconductor · synthetic methods

[1] A. Shimizu, R. Kishi, M. Nakano, D. Shiomi, K. Sato, T. Takui, I. Hisaki, M. Miyata, Y. Tobe, *Angew. Chem. Int. Ed.* **2013**, *52*, 6076–6079; *Angew. Chem.* **2013**, *125*, 6192–6195.
[2] J. J. Dressler, Z. Zhou, J. L. Marshall, R. Kishi, S. Takamuku, Z. Wei, S. N. Spisak, M. Nakano, M. A. Petrukhina, M. M. Haley, *Angew. Chem. Int. Ed.* **2017**, *56*, 15363–15367; *Angew. Chem.* **2017**, *129*, 15565–15569.
[3] C. K. Frederickson, B. D. Rose, M. M. Haley, *Acc. Chem. Res.* **2017**, *50*, 977–987.
[4] A. G. Fix, P. E. Deal, C. L. Vonnegut, B. D. Rose, L. N. Zakharov, M. M. Haley, *Org. Lett.* **2013**, *15*, 1362–1365.
[5] B. D. Rose, L. E. Shoerb, M. R. Wasielewski, M. M. Haley, *Chem. Phys. Lett.* **2014**, *616–617*, 137–141.
[6] P. Hu, S. Lee, T. S. Herng, N. Aratani, T. P. Gonçalves, Q. Qi, X. Shi, H. Yamada, K. Huang, J. Ding, D. Kim, J. Wu, *J. Am. Chem. Soc.* **2016**, *138*, 1065–1077.
[7] J. J. Dressler, M. M. Haley, *J. Phys. Org. Chem.* **2020**, *33*, e4114.
[8] Z. Zeng, X. Shi, C. Chi, J. T. López Navarrete, J. Casado, J. Wu, *Chem. Soc. Rev.* **2015**, *44*, 6578–6596.
[9] X. Fu, H. Han, D. Zhang, H. Yu, Q. He, D. Zhao, *Chem. Sci.* **2020**, *11*, 5565–5571.
[10] C. K. Frederickson, J. E. Barker, J. J. Dressler, Z. Zhou, E. R. Hanks, J. P. Bard, L. N. Zakharov, M. A. Petrukhina, M. M. Haley, *Synlett* **2018**, *29*, 2562–2566.
[11] K. Fukuda, T. Nagami, J. Fujiyoshi, M. Nakano, *J. Phys. Chem. A* **2015**, *119*, 10620–10627.
[12] G. E. Rudebusch, J. L. Zafra, K. Jorner, K. Fukuda, J. L. Marshall, I. Arrechea-Marcos, G. L. Espejo, R. P. Ortiz, C. J. Gómez-García, L. N. Zakharov, M. Nakano, H. Ottosson, J. Casado, M. M. Haley, *Nat. Chem.* **2016**, *8*, 753–759.
[13] D. T. Chase, A. G. Fix, S. J. Kang, B. D. Rose, C. D. Weber, Y. Zhong, L. N. Zakharov, M. C. Lonergan, C. Nuckolls, M. M. Haley, *J. Am. Chem. Soc.* **2012**, *134*, 10349–10352.
[14] Z. Wang, Y. Dai, L. Ding, B. Dong, S. Jiang, J. Wang, J. Pei, *Angew. Chem. Int. Ed.* **2021**, *60*, 4594–4598; *Angew. Chem.* **2021**, *133*, 4644–4648.
[15] A. M. Zeidell, L. Jennings, C. K. Frederickson, Q. Ai, J. J. Dressler, L. N. Zakharov, C. Risko, M. M. Haley, O. D. Jurchescu, *Chem. Mater.* **2019**, *31*, 6962–6970.
[16] G. E. Rudebusch, G. L. Espejo, J. L. Zafra, M. Peña-Alvarez, S. N. Spisak, K. Fukuda, Z. Wei, M. Nakano, M. A. Petrikhina, J. Casado, M. M. Haley, *J. Am. Chem. Soc.* **2016**, *138*, 12648–12654.
[17] X. Ji, T. Huang, W. Wu, F. Liang, S. Cao, *Org. Lett.* **2015**, *17*, 5096–5099.
[18] X. Xu, Y. Yao, B. Shan, X. Gu, D. Liu, J. Liu, J. Xu, N. Zhao, W. Hu, Q. Miao, *Adv. Mater.* **2016**, *28*, 5276–5283.
[19] H. Hayashi, J. E. Barker, A. C. Valdivia, R. Kishi, S. N. MacMillan, C. J. Gómez-García, H. Miyauchi, Y. Nakamura, M. Nakano, S.-I. Kato, M. M. Haley, J. Casado, *J. Am. Chem. Soc.* **2020**, *142*, 20444–20455.

Manuscript received: January 29, 2021
Accepted manuscript online: April 8, 2021
Version of record online: June 4, 2021